Boundary-Layer Meteorol (2011) 140:225–241
DOI 10.1007/s10546-011-9606-4

ARTICLE

Comparing Two Implementations of a Micromixing Model. Part II: Canopy Flow

John V. Postma · John D. Wilson · Eugene Yee

Received: 29 September 2010 / Accepted: 11 March 2011 / Published online: 12 April 2011

Abstract The sequential particle micromixing model (SPMMM) is used to estimate concentration fluctuations in plumes dispersing into a canopy flow. SPMMM uses the familiar single-particle Lagrangian stochastic (LS) trajectory framework to pre-calculate the required conditional mean concentrations, which are then used by an interaction by exchange with the conditional mean (IECM) micromixing model to predict the higher-order fluctuations of the scalar concentration field. The predictions are compared with experimental wind-tunnel dispersion data for a neutrally stratified canopy flow, and with a previously reported implementation using simultaneous particle trajectories. The two implementations of the LS–IECM model are shown to be largely consistent with one another and are able to simulate dispersion in a canopy flow with fair to good accuracy.

Keywords Canopy flow · Concentration fluctuations · Micromixing modelling · Scalar dissipation

1 Introduction

The state variable $(\boldsymbol{X}, \boldsymbol{U})$ in a first-order Lagrangian stochastic (LS) trajectory model comprises the position and velocity of a fluid element, and may be augmented to include the concentration ϕ of some gas of interest, this being computed using a micromixing model. SPMMM is the acronym—it stands for sequential particle micromixing model—given by Postma et al. (2011, hereafter referred to as Part I) to their particular implementation of a standard LS model coupled to the interaction by exchange with the conditional mean (IECM) micromixing model (Fox 1996; Pope 1998). Here, we extend to more complex flows our

J. V. Postma (✉) · J. D. Wilson
Department of Earth and Atmospheric Sciences, University of Alberta, Edmonton, AB T6G 2E3, Canada
e-mail: jpostma@ualberta.ca

E. Yee
Defence R&D Canada-Suffield, P.O. Box 4000, Medicine Hat, AB T1A 8K6, Canada

earlier comparison with an alternative *implementation* of the same LS and micromixing models by Cassiani et al. (2005, hereafter referred to as the CASS model or implementation).

The coupling of the LS model and the IECM micromixing model allows SPMMM and the CASS model to predict the higher-order moments of the scalar concentration field. We emphasize at the outset that SPMMM and the CASS model are mathematically equivalent, but differ in their numerical implementation. Both release N independent particles to compute the required conditional mean concentrations. However, while the CASS implementation computes the trajectories of the N particles simultaneously, calculating the conditional mean concentrations at each timestep (or 'on-the-fly'), SPMMM computes the trajectories of the N particles *sequentially* and pre-calculates the needed conditional mean concentrations. In both implementations, the trajectories of the particles are computed with single-point velocity statistics.

In Part I, SPMMM was used to simulate dispersion in a wall shear layer. As conveniently simple and comprehensible as a wall shear layer is, its occurrence outside of wind tunnels and water channels is rare. The surface of the earth is for the most part neither flat nor uniform. It is covered with different types of vegetation and buildings of different shapes which collectively make up the canopy. In the case of a city, over small distances, the individual canopy elements change rapidly as we pass over parks, downtown cores, and residential areas. There are, however, also large areas where the canopy is approximately uniform. Modern suburban areas, for example, have row upon row of similarly shaped and sized houses, and many forests contain very similarly aged and sized trees. Perhaps the most uniform canopy can be found in crops, a monoculture of equally aged and uniformly spaced plants, such as a cornfield. As the majority of the human population resides in areas covered by some form of canopy, a model that can accurately simulate dispersion within in a canopy would be of great benefit for emergency preparedness and urban planning (nuisance odours). Furthermore, the use of chemical fertilizers and pesticides may be reduced with a more thorough understanding of dispersion through the crop canopy.

The principal advantage of the sequential particle/pre-calculation architecture of SPMMM over the simultaneous particle/on-the-fly architecture of the CASS model is the potential for very fast simulations, since SPMMM can be trivially parallelized due to the independent nature of the particles (in that they are released one at a time, rather than simultaneously). In the CASS implementation, the conditional mean concentrations are calculated based on the concentrations and velocities of the particles that occupy a particular region of space. In a parallel-computing environment, communication between the processors takes time: to calculate the conditional mean concentrations, the program must pause, share particle position, velocity, and concentration information amongst the processors, perform the calculations and then carry on to the next timestep. Modern parallel algorithms utilizing domain decomposition can attain approximately 80% parallel efficiency (e.g. Rembold et al. 2008), but the sequential particle/pre-calculation framework of SPMMM allows for trivial computational parallelization and an almost linear increase in performance. The drawback is that it cannot be used to simulate the dispersion of chemically reactive species.

The simulation of chemical reactions requires at the very least the concentrations of all species to be known. This is not possible with SPMMM, since a single particle at a time is used to pre-calculate the conditional mean concentrations—at the most one species could be simulated. In the CASS implementation, the N particles are released simultaneously and could (if desired) represent different chemical species. At each timestep, the concentrations of each species could be calculated and the reaction simulated.

Decreased simulation times are particularly advantageous for emergency preparedness scenarios—a chemical spill in a densely populated urban centre, for example. In this case,

emergency responders would benefit greatly from a model that can quickly and accurately predict the resulting plume, thus allowing for the evacuation of threatened populations. Furthermore, a model that provides a more complete picture of the concentration field (by predicting higher-order moments) would allow responders to more accurately predict dosage and exposure of any population who could not be evacuated in time.

It was shown in Cassiani et al. (2007) that the parametrization of the micromixing time scale used in both SPMMM and the CASS models performed well for simulating dispersion in a canopy flow with the simultaneous particle/on-the-fly implementation of the CASS model. In this article, we investigate whether this is also true for the sequential particle/precalculation implementation of SPMMM.

2 Model Formulation

A full description of SPMMM can be found in Part I, and so we provide a summary only of the relevant equations and their numerical implementation.

2.1 Governing Equations

The equations that govern the evolution of the velocity, position and concentration of a marked fluid element are, respectively:

$$\mathrm{d}U_i' = a_i(\boldsymbol{X}, \boldsymbol{U}', t)\mathrm{d}t + b_{ij}(\boldsymbol{X}, \boldsymbol{U}', t)\mathrm{d}\xi_j(t), \tag{1}$$

$$\mathrm{d}X_i = \left(\langle u_i \rangle + U_i'\right)\mathrm{d}t, \tag{2}$$

$$\mathrm{d}\phi = -\frac{1}{t_\mathrm{m}}(\phi - \langle \phi | \boldsymbol{u} \rangle)\mathrm{d}t, \tag{3}$$

where U_i' is the Lagrangian velocity fluctuation relative to the Eulerian mean (viz., $U_i' = u_i - \langle u_i \rangle$), X_i is the particle position, ϕ is the scalar concentration, $\mathrm{d}t$ is a small timestep and $\mathrm{d}\xi_j(t)$ represents an incremental Wiener process with zero mean and variance $\mathrm{d}t$. On the right-hand side of Eq. 1, we have the deterministic drift term $a_i\mathrm{d}t$, and the stochastic diffusion term $b_{ij}\mathrm{d}\xi_j$. In Eq. 3, we have the scalar micromixing time scale t_m, and the mean scalar concentration conditioned on the local velocity $\langle \phi | \boldsymbol{u} \rangle$ (also called the conditional mean concentration).

Following the lead of Thomson (1987), we specify the form of the probability density function (PDF) of the Eulerian velocity fluctuations to be a stationary Gaussian:

$$g_\mathrm{a}(\boldsymbol{x}, \boldsymbol{u}') = \frac{[\det(R^{-1})]^{1/2}}{(2\pi)^{3/2}} \exp\left(-\frac{1}{2}u_i' R_{ij}^{-1} u_j'\right), \tag{4}$$

where $R_{ij} = \langle u_i' u_j' \rangle$ is the Reynolds stress tensor and R_{ij}^{-1} is its inverse. Using the well-mixed condition (Thomson 1987), a particular functional form for a_i is obtained:

$$a_i = T_i^{(0)} + T_{ij}^{(1)} U_j' + T_{ijk}^{(2)} U_j' U_\mathrm{k}', \tag{5}$$

with

$$T_i^{(0)} \equiv \frac{1}{2}\frac{\partial R_{i\ell}}{\partial x_\ell}, \tag{6}$$

$$T_{ij}^{(1)} \equiv -\frac{1}{2}(C_0\varepsilon)R_{ij}^{-1} + \frac{1}{2}R_{j\ell}^{-1}\frac{\partial R_{i\ell}}{\partial x_\mathrm{k}}\langle u_\mathrm{k}\rangle$$

$$= -\frac{1}{2}(C_0\varepsilon)R_{ij}^{-1} + T_{ijk}^{(2)}\langle u_\mathrm{k}\rangle, \tag{7}$$

$$T_{ijk}^{(2)} \equiv \frac{1}{2}R_{j\ell}^{-1}\frac{\partial R_{i\ell}}{\partial x_\mathrm{k}}, \tag{8}$$

where C_0 is the universal Kolmogorov constant, ε is the turbulent kinetic energy (TKE) dissipation rate and $\langle u_\mathrm{k}\rangle$ is the mean Eulerian velocity. By specifying

$$b_{ij} = \delta_{ij}(C_0\varepsilon)^{1/2}, \tag{9}$$

as the form of the stochastic term coefficient in Eq. 1, consistency of the LS model with Kolmogorov's theory of local isotropy (Monin and Yaglom 1975) is assured.

2.2 Parametrization of the Micromixing Time Scale

SPMMM uses a parametrization for the micromixing time scale first proposed by Cassiani et al. (2005) for non-homogeneous, non-isotropic turbulence, where local equilibrium and local isotropy are assumed:

$$t_\mathrm{m} = \mu\left(\frac{\sigma_\mathrm{r}^2}{\sigma_{U_\mathrm{r}}^2}\right)^{1/2}. \tag{10}$$

The micromixing constant, μ, is effectively a 'tuning' parameter that depends upon the type of turbulence, the source configuration, and the stage of development of the plume. The instantaneous plume width is denoted by σ_r and the variance of the Lagrangian relative velocity fluctuations by $\sigma_{U_\mathrm{r}}^2$. This variance was modelled (Franzese 2003; Cassiani et al. 2005) as

$$\sigma_{U_\mathrm{r}}^2 = \sigma^2\left(\frac{\sigma_\mathrm{r}}{L}\right)^{2/3}, \tag{11}$$

where

$$L = \frac{(3\sigma^2/2)^{3/2}}{\varepsilon}, \tag{12}$$

represents the length scale of the most energetic eddies, and

$$\sigma^2 = \frac{\sigma_u^2 + \sigma_v^2 + \sigma_w^2}{3} = \frac{2k}{3}, \tag{13}$$

where the streamwise, spanwise and vertical velocity variances are denoted by σ_u^2, σ_v^2 and σ_w^2, respectively, and the TKE is denoted by k. Wherever $\sigma_\mathrm{r} > L$, the constraint $\sigma_{U_\mathrm{r}}^2 = \sigma^2$ is imposed. The instantaneous plume width is modelled as

$$\sigma_\mathrm{r}^2 = \frac{d_\mathrm{r}^2}{1 + (d_\mathrm{r}^2 - \sigma_0^2)/(\sigma_0^2 + 2\sigma^2 T_L t)}, \tag{14}$$

where d_r is the root-mean-square separation between particle pairs in the instantaneous plume and calculated in accordance with the Richardson law:

$$d_r^2 = C_r \varepsilon (t + t_0)^3, \tag{15}$$

where C_r is the Richardson constant, and $T_L \equiv 2\sigma^2/(C_0\varepsilon)$ is the Lagrangian integral time scale. By invoking linearization, this equation is discretized as

$$d_r^2(t + \Delta t) = d_r^2(t) + 3C_r \varepsilon (t + t_0)^2 \Delta t, \tag{16}$$

with the constraint that $\sigma_r^2(t+\Delta t) \geq \sigma_r^2(t)$. The constant $t_0 = t_s/C_r^{1/3}$ (where $t_s = (\sigma_0^2/\varepsilon)^{1/3}$ is the characteristic time scale of the source, and σ_0 is the initial source distribution) ensures that $t_m \to t_s$ as $t \to 0$.

2.3 Numerical Implementation

Before simulating micromixing, SPMMM requires the conditional mean concentration field $\langle \phi | \boldsymbol{u} \rangle$ that is pre-calculated by the program MEANS. To maximize model resolution, the calculation of the conditional mean concentration field is performed on a dynamic grid that encompasses the plume in both the spatial (x, y, z) and velocity (u, v, w) domains, similar to the technique employed by the CASS model. The spatial domain is discretized into N_x streamwise bins, N_y spanwise bins and N_z vertical bins, while the velocity domain is discretized into N_u streamwise velocity bins, N_v spanwise velocity bins and N_w vertical velocity bins. The position and velocity of the particle are indexed in discretized space as $(x_I, y_J, z_K, u_L, v_M, w_N)$, where upper-case subscripts are used to denote this discretization. All calculations by MEANS and SPMMM are performed on this grid. As in Part 1, a forward difference scheme was used to solve Eqs. 1 and 2.

MEANS calculates the conditional mean concentrations by releasing from the source region N_ϕ particles, one at a time, and accumulating conditional residence times $t_r^v = t_r^v(x_I, y_J, z_K, u_L, v_M, w_N)$ for each bin in position–velocity space. From these residence times, the conditional mean concentration field is calculated as

$$\langle \phi | \boldsymbol{u} \rangle = \langle \phi | \boldsymbol{u} \rangle (x_I, y_J, z_K, u_L, v_M, w_N) = \frac{Q t_r^v}{\mathscr{V} N_\phi^v}, \tag{17}$$

where

$$N_\phi^v = N_\phi^v(x_I, y_J, z_K, u_L, v_M, w_N) = N_\phi f_{\mathbf{u}} \Delta u \Delta v \Delta w, \tag{18}$$

is the number of particles during the simulation that visit bin $(x_I, y_J, z_K, u_L, v_M, w_N)$, Q is the source strength, $\mathscr{V} = \mathscr{V}(x_I, y_J, z_K)$ is the volume of a spatial bin and $f_{\mathbf{u}}$ is the PDF of the driving velocity statistics.

The algorithm for calculating the micromixing time scales is very similar to that outlined in Cassiani et al. (2005, 2007). SPMMM calculates $t_m(x_I, y_J, z_K)$ before simulating mixing by releasing a small sub-ensemble of particles sequentially from the source region. The micromixing time scale for the particle is computed according to Eqs. 10–16. When the last of the particles in the sub-ensemble has exited the spatial domain through $x > x_{max}$, the mean micromixing time scale in bin (x_I, y_J, z_K) is calculated. For regions outside of the plume, the micromixing time scale is equal to the turbulence time scale $\tau = k/\varepsilon$. Furthermore, if $t_m > \tau$, then t_m is reset to τ.

In the micromixing stage of the simulation, N particles are released sequentially from the upstream face of the spatial domain. They are initialized uniformly on this face and their

initial concentration depends upon whether they are released from a source or non-source region. If the particle originates within the SPMMM source region, then it is given an initial concentration of $\phi_0 = \phi_{\text{src}}$, where ϕ_{src} is the source concentration; otherwise, it is given an initial concentration of $\phi_0 = 0$. The source configuration was chosen to be an infinite line along the y-axis with a source height of z_{s}. The initial distribution was modelled as a Gaussian along the z-axis. The source concentration profile is thus

$$\phi_{\text{src}} = \frac{Q}{\sqrt{2\pi}\sigma_0 U} \exp\left(\frac{-(z - z_{\text{s}})^2}{2\sigma_0^2}\right). \tag{19}$$

Since virtually all of the particles in the MEANS simulations would have been initialized within five standard deviations of the source height, a particle is considered to be in the SPMMM source region if $|z - z_{\text{s}}| \leq 5\sigma_0$. However, beyond $|z - z_{\text{s}}| \approx 3\sigma_0$, Eq. 19 gives $\phi_{\text{src}} \approx 0$. The concentration of the particle is compared with the conditional mean concentration for the position–velocity bin that it currently occupies as it travels downstream, and is updated according to

$$\phi(t + \Delta t) = \phi(t) \exp(-\Delta t / t_{\text{m}}) + \langle \phi | \boldsymbol{u} \rangle (1 - \exp(-\Delta t / t_{\text{m}})). \tag{20}$$

Position and concentration data of the particles are extracted at user-specified planes and saved for post-processing.

The timestep for the micromixing stage of SPMMM is

$$\Delta t = \mu_t \min[T_{L_u}, T_{L_v}, T_{L_w}, t_{\text{m}}], \tag{21}$$

where $\mu_t \ll 1$ is the timestep constant and the Lagrangian integral time scales associated with the streamwise, spanwise and vertical velocities are calculated as

$$T_{L_u} = \frac{2\sigma_u^2}{C_0 \varepsilon}, \tag{22a}$$

$$T_{L_v} = \frac{2\sigma_v^2}{C_0 \varepsilon}, \tag{22b}$$

$$T_{L_w} = \frac{2\sigma_w^2}{C_0 \varepsilon}. \tag{22c}$$

The timestep used in MEANS for computation of the conditional mean concentrations and in SPMMM for determination of the micromixing time scale was $\Delta t = \mu_t \min[T_{L_u}, T_{L_v}, T_{L_w}]$.

Perfectly reflective boundary conditions were employed on the upstream, top and bottom faces of the simulation domain. Periodic boundary conditions were used on the lateral faces. Neither SPMMM nor the CASS model resolve the canopy obstacles. Therefore, no reflection scheme was needed to model the interaction of particles and the canopy obstacles.

3 Experimental and Computational Set-up

3.1 The Tombstone Canopy Experiments

The Tombstone Canopy consisted of a regular diamond-shaped array of thin billboard-like obstacles. Each obstacle was a rectangular aluminum tab measuring 10 mm in spanwise width, 1 mm in streamwise thickness, and $h_{\text{c}} = 60$ mm in height. The centre-to-centre streamwise and spanwise spacings of the tabs were 44 and 60 mm, respectively. A neutral boundary layer

was grown over a rough surface (consisting of gravel) within the Commonwealth Scientific and Industrial Research Organization (CSIRO) Pye Laboratory open–return blower tunnel and then encountered the Tombstone Canopy, which extended for 3 m in the streamwise direction and covered the entire span of the wind tunnel. Velocity statistics for the u and w components were extracted using a three-element hot-wire anemometer and a miniature one-component sonic anemometer. The turbulence structure within and above the canopy is described in Raupach et al. (1986).[1] The boundary-layer depth was $\delta = 540\,\mathrm{mm}$, and the free-stream velocity was $\langle u\rangle_\delta = 11.25\,\mathrm{m\,s^{-1}}$. The Reynolds number for the flow (based on δ and $\langle u\rangle_\delta$) was $\mathrm{Re}_\delta \approx 4.0 \times 10^5$. The friction velocity based on spatially averaged measurements just above the canopy was $u_* = 1.03\,\mathrm{m\,s^{-1}}$, the roughness length was $z_0 = 8.3\,\mathrm{mm}$, and the spatially averaged mean streamwise velocity at canopy height was $\langle u\rangle_\mathrm{c} = 3.40\,\mathrm{m\,s^{-1}}$. Based on $\langle u\rangle_\mathrm{c}$ and h_c, the Reynolds number was $\mathrm{Re}_\mathrm{c} \approx 1.4 \times 10^4$.

Two sets of dispersion experiments were carried out in the Tombstone Canopy flow: from an elevated plane source (Coppin et al. 1986); and from an elevated cross-wind line source (Legg et al. 1986). Here, we focus on the results for the elevated line source. The source in the continuous, cross-wind, elevated line source experiments was a 0.9 mm diameter hot wire positioned at a height of $z_\mathrm{s} = 0.85h_\mathrm{c} = 51\,\mathrm{mm}$, and placed midway between two rows of obstacles. The source strength varied in the range, $Q = 60 - 350\,\mathrm{W\,m^{-1}}$ from experiment to experiment. The heat generated by the wire was sufficiently so low that it did not alter the turbulence structure and could be treated as a passive tracer, allowing the temperature fluctuations to be interpreted as concentration fluctuations. Concentration statistics were extracted with a cold-wire resistance thermometer and made dimensionless with

$$\phi_* = \frac{Q}{\rho c_\mathrm{p} z_\mathrm{s} \langle u\rangle_\mathrm{s}}, \tag{23}$$

where ρ is the density of air, c_p is the heat capacity of air at constant pressure and $\langle u\rangle_\mathrm{s}$ is the mean streamwise velocity at source height.

3.2 Driving Velocity Statistics and the TKE Dissipation Rate

Recall from Part I that SPMMM requires driving velocity statistics and a TKE dissipation rate. Figure 1 displays polynomial interpolations to the data presented in Fig. 6 of Raupach et al. (1986, 1987). They are identical to those used by Cassiani et al. (2007) to drive their model, so that a direct comparison of the two models can be made. Since the Raupach et al. (1986) velocity data did not include any v-component measurements, the standard deviation of the spanwise velocity was estimated as $\sigma_v^2 = (\sigma_u^2\sigma_w^2)^{1/2}$, as suggested by Brunet et al. (1994), and used by Cassiani et al. (2007). The velocity statistics were assumed to be horizontally homogeneous and stationary. We note that the presence of the canopy in the SPMMM simulations is manifested through its effects on the driving velocity statistics and the TKE dissipation rate.

The left panel of Fig. 2 shows the polynomial fit to the far-field Lagrangian integral time scale from Fig. 10 of Legg et al. (1986), where it was assumed that the Lagrangian vertical velocity autocorrelation function had an exponential form, and that the variances of Eulerian and Lagrangian vertical velocities were equal, which is strictly true only in homogeneous turbulence. Consequently, the profile is meant to provide some indication of the behaviour of T_L, and not represent it exactly. No measurements of T_L were made above $3h_\mathrm{c}$; above this height, the value is held constant. The right panel of Fig. 2 shows three different determinations of

[1] There were two errors in the axes labels of Fig. 6 in Raupach et al. (1986). The figure is corrected in Raupach et al. (1987).

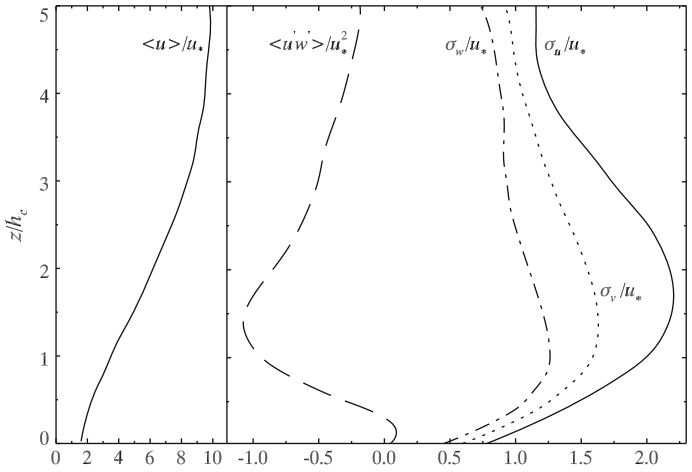

Fig. 1 Vertical profiles of the dimensionless velocity statistics for the Tombstone Canopy flow. The *left panel* shows the dimensionless streamwise mean velocity. In the *right panel*, the various lines display (from *right* to *left*): the dimensionless standard deviation of the streamwise velocity σ_u/u_* (*solid line*); the dimensionless standard deviation of the spanwise velocity σ_v/u_* (*dotted line*); the dimensionless standard deviation of the vertical velocity σ_w/u_* (*dot-dashed line*); and the dimensionless covariance $\langle u'w'\rangle/u_*^2$ (*dashed line*). The velocity statistics were assumed to be horizontally homogeneous and stationary

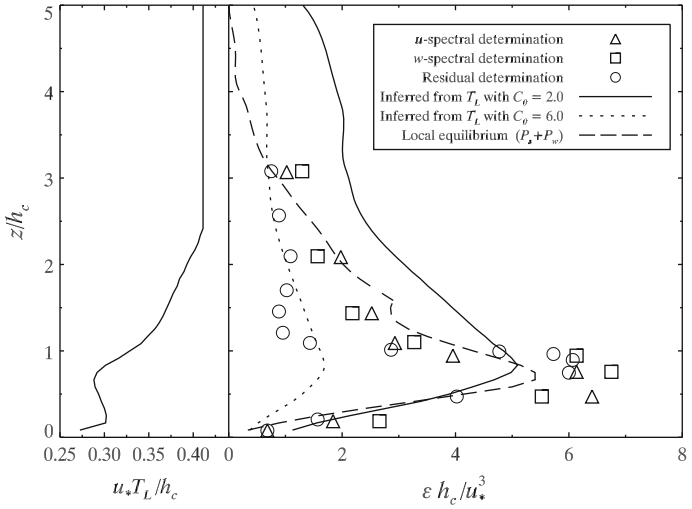

Fig. 2 Vertical profiles of the dimensionless Lagrangian integral time scale (*left panel*) and dimensionless TKE dissipation rates (*right panel*) for the Tombstone Canopy flow. Several different determinations (both measured and modelled) of the TKE dissipation rate are shown in the right panel: u-spectral determination (*triangles*); w-spectral determination (*squares*); residual determination (*circles*); inferred from the T_L profile with $C_0 = 2.0$ (*solid line*); inferred from the T_L profile with $C_0 = 6.0$ (*dotted line*); and by assuming local equilibrium (*dashed line*)

the TKE dissipation rate from Fig. 15 of Raupach et al. (1986): from the u-velocity spectra (triangles); from the w-velocity spectra (squares); and from a residual calculation (circles) in accordance with

$$\varepsilon = P_\mathrm{s} + P_w + T_\mathrm{t}, \tag{24}$$

where

$$P_\mathrm{s} = -\langle u'w' \rangle \frac{\partial \langle u \rangle}{\partial z}, \tag{25}$$

is the shear production,

$$P_w = -\langle u \rangle \frac{\partial \langle u'w' \rangle}{\partial z}, \tag{26}$$

is the wake production, and T_t is the turbulent transport (which does not have a closed form). The three measurements agree reasonably well within the canopy but display a factor of two discrepancy between the spectral and residual methods above the canopy.

Cassiani et al. (2007) interpreted the Lagrangian integral time scale measurements of Legg et al. (1986) to be T_{L_w} and used the relation $T_{L_w} = 2\sigma_w^2 / C_0 \varepsilon$ to determine the TKE dissipation rate. They found that $C_0 = 2.0$ produced an acceptable fit to the measured TKE dissipation data, as shown by the solid line in the right panel of Fig. 2. The value of $C_0 = 2$ lies at the lower end of the currently accepted range of values for this parameter, and is substantially different than $C_0 = 6$ used in the wall shear-layer simulations in Part I. However, the TKE dissipation rate inferred from T_L with $C_0 = 6.0$ does not fit any of the in-canopy TKE dissipation measurements very well, as shown by the dotted line in Fig. 2.

A second method of calculating the TKE dissipation rate uses Eq. 24. Since the shear and wake productions of TKE are in closed form, they are readily calculated from the available velocity statistics. However, the turbulent transport of TKE is unclosed and must be modelled, which has the undesirable side-effect of introducing more arbitrary constants into the estimation of ε, and thus into SPMMM. We therefore chose simplicity, and assumed local equilibrium, and calculated the TKE dissipation rate as $\varepsilon \approx P_\mathrm{s} + P_w$. A Savitzky–Golay filter was used to remove noise from the profile. The resulting profile is shown by the dashed line in Fig. 2. Overall, this method produced a good fit to the experimental data, and is slightly better than the method of inferring a TKE dissipation rate from a profile of the Lagrangian integral time scale, particularly above the canopy. Furthermore, it does so with no reference to (or dependence upon a chosen value of) the Kolmogorov constant. The assumption of local equilibrium within the canopy is certainly incorrect. Raupach et al. (1986) note that turbulent transport was a major loss in the TKE budget just above the canopy and was the principal gain within the upper canopy. Thus, the inclusion of T_t in the calculation of the TKE dissipation rate would probably result in a better fit to the experimental data. However, as shown in Fig. 2, the assumption of local equilibrium can be used to determine a reasonably accurate TKE dissipation rate, without the need for introducing further tunable parameters into the estimation scheme for ε.

3.3 Set-up for the SPMMM Simulations

In this article, we compare two SPMMM simulations of dispersion of a passive scalar from a continuous, elevated, cross-wind line source into the Tombstone Canopy flow with the simulation results of Cassiani et al. (2007). One simulation used a TKE dissipation rate inferred from the T_L profile (hereafter called SPMMM–ID, for *inferred dissipation*), and the other used a TKE dissipation rate calculated assuming local equilibrium (hereafter called SPMMM–LD, for *local dissipation*).

Table 1 Summary of the SPMMM simulations used for this study

Run	C_0	TKE dissipation rate	C_r	μ
SPMMM–ID	2.0	Inferred from T_L	0.12	0.82
SPMMM–LD	6.0	Local equilibrium	0.45	0.75

In Part I, the micromixing model parameters had been optimized to $\mu = 0.75$ and $C_r = 0.45$, and the Kolmogorov constant to $C_0 = 6.0$, by simulating dispersion from an elevated compact source in the Fackrell and Robins (1982) wall shear-layer flow. As discussed in Thomson (1996), Sawford (2004), and Luhar and Sawford (2005), the micromixing constant will be larger for a line source than for a compact source since mixing is more efficient for a compact source plume. This is because, for a line source, plume entrainment only occurs in the vertical direction as opposed to the spanwise and vertical directions for a point-source plume. Investigation showed that increasing the micromixing model constant to $\mu = 0.80 - 0.85$ resulted in a slightly better fit to the experimental data above the height of the maximum concentration standard deviation, and a slightly poorer fit below. Overall, the performance measures did improve slightly upon increasing μ, but the difference was not marked, so we will continue to use $\mu = 0.75$, $C_r = 0.45$, and $C_0 = 6.0$ for the SPMMM–LD simulation to avoid arbitrarily re-tuning the constants.

The SPMMM–ID simulation was meant to provide a more direct comparison between the CASS model and SPMMM. The Kolmogorov constant was set to $C_0 = 2.0$, as this value produced the best fit to the measured TKE dissipation rate (as shown in Fig. 2), and was the value used in Cassiani et al. (2007). Based on the theoretical study of Franzese and Cassiani (2007), Cassiani et al. (2007) noted that, for a smaller C_0, a proportionally smaller C_r must be used. The value of C_r was not explicitly stated in their article, and so we interpreted their statement to imply direct proportionality between C_r and C_0. Thus, we assumed that Cassiani et al. (2007) used $C_r = 0.12$ (viz., $C_r/C_0 = 0.3/5 = 0.12/2$). This honours the proportionality for homogeneous isotropic turbulence derived in Franzese and Cassiani (2007), but does not use the exact expression ($C_r \approx C_0/11$). The micromixing constant was set to $\mu = 0.82$ in Cassiani et al. (2007). Therefore, the parameters for the SPMMM–ID simulation were $\mu = 0.82$, $C_r = 0.12$ and $C_0 = 2.0$. Table 1 summarizes the parameters used in the SPMMM simulations.

For both SPMMM simulations, the spatial domain was discretized into 60 bins in the x, y and z directions: $N_x = 60$, $N_y = 60$ and $N_z = 60$. The conditional mean concentrations were calculated in a velocity domain that was discretized into 20 bins in the u, v and w directions: $N_u = 20$, $N_v = 20$ and $N_w = 20$. The timestep constant was $\mu_t = 0.02$. As for the wall shear-layer simulations in Part I, the canopy flow simulations showed little sensitivity to the streamwise spatial resolution. First-order consistency between MEANS and SPMMM was realized at this velocity resolution since the driving velocity statistics shown in Fig. 1 are smoothly varying with low complexity.

The use of a continuous line source effectively reduces the simulations to two dimensions allowing the use of fewer particles. To pre-calculate the conditional mean concentration field with MEANS, we used $N_\phi = 2 \times 10^6$ particles. Similarly, since in a line source simulation there is a much greater chance of a particle being a source particle in SPMMM, we used $N = 5 \times 10^6$ particles. An initial source distribution with $\sigma_0 = 2.0 d_s$ was found to produce the best fit to the experimental measurements of the standard deviation of concentration close to the source.

4 Simulation Results

As in Part I, three performance measures are used to evaluate the SPMMM simulations, namely, the fractional bias:

$$FB = \frac{(\overline{Q_o} - \overline{Q_p})}{0.5(\overline{Q_o} + \overline{Q_p})}, \tag{27}$$

the normalized mean-square error:

$$NMSE = \frac{\overline{(Q_o - Q_p)^2}}{\overline{Q_o}\ \overline{Q_p}}, \tag{28}$$

and the fraction of data within a factor of 2 of the observations:

$$FAC2 = \text{fraction of data that satisfy } 0.5 \leq \frac{Q_p}{Q_o} \leq 2.0. \tag{29}$$

In these definitions, an observed quantity (wind-tunnel data) is denoted by Q_o, and a predicted quantity (SPMMM model result) is denoted by Q_p. An overbar indicates an arithmetic mean of all (or some subset of) the available observations or predictions. Chang and Hanna (2004) suggest that, for an acceptable model, the performance measures should satisfy $-0.3 < FB < 0.3$, $0 \leq NMSE < 4$, and $FAC2 > 0.5$.

Figure 3 displays the vertical profile of the dimensionless mean concentration at three downstream positions. Qualitatively, the simulation matches the experimental data reasonably well. At all the three locations, SPMMM produced profiles with a similar shape and magnitude to the experimental data. For the three simulations, the agreement is better above the canopy than below at the three downstream locations. This may be related to the Kolmogorov constant, as it is the only tunable parameter in SPMMM, which affects the mean concentration. Since the parametrization of micromixing timescale is based on inertial-subrange theory, and canopy flow lacks a well-defined inertial subrange, it is likely that the improved performance of the SPMMM–ID simulation may simply be due to a compensation for the intricacies of canopy flow by a reduction of the Kolmogorov constant.

Poggi et al. (2008) investigated the behaviour of C_0 inside dense canopies. They found that C_0 is reduced by a factor of $\approx$5 relative to its atmospheric surface layer value due to wake production, and a factor of $\approx$1.5 due to finite Reynolds number effects. These reductions were offset by an increase in C_0, due to a short circuiting of the energy cascade within the canopy, but not sufficient to compensate for the reductions. Indeed, the SPMMM–ID and the Cassiani et al. (2007) simulation results (both of which utilized $C_0 = 2.0$) display better agreement with the experimental data within the canopy. The agreement between these two simulations is also quite good. The SPMMM–LD simulations show the poorest agreement with the experimental data, with the largest below canopy underprediction at $x/h_c = 2.78$ and the largest within canopy overprediction at $x/h_c = 11.6$. However, in another SPMMM–LD simulation where $C_0 = 4.0$ (not shown), the below canopy height agreement of the simulated and the experimental vertical profiles of mean concentration was much improved, further supporting the findings of Poggi et al. (2008).

Part of the below-canopy discrepancy in all the three models may also be partly because neither the SPMMM nor the CASS implementation resolves the canopy obstacles. Consider a scenario where reflection of a particle off of the upstream face of a canopy obstacle occurs. After reflection, there could be a short period of upstream motion before the particle is caught up in mean streamwise flow and begins moving downstream again. This upstream motion

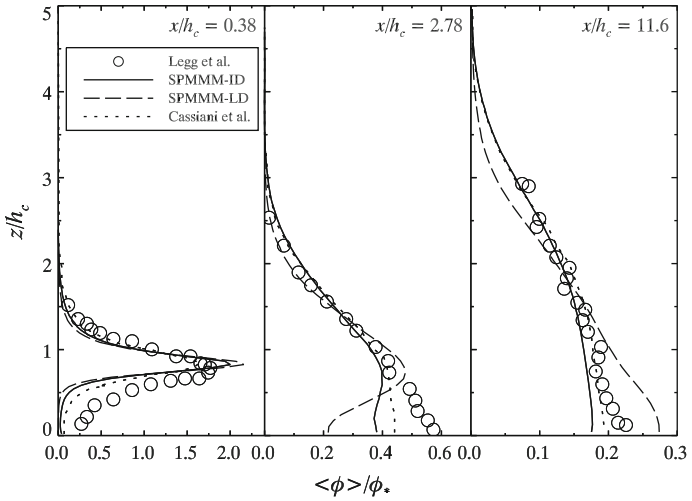

Fig. 3 Measured and modelled vertical profiles of the dimensionless mean concentration resulting from dispersion from a continuous, cross-wind line source ($z_s/h_c = 0.85$) in the Tombstone Canopy flow. The *circles* represent measurements from Legg et al. (1986). Three simulated profiles are shown: an SPMMM simulation utilizing a TKE dissipation rate inferred from T_L (*solid lines*), an SPMMM simulation utilizing a TKE dissipation rate calculated assuming local equilibrium (*dashed lines*), and the results of the Cassiani et al. (2007) model (*dotted lines*), which also used an inferred TKE dissipation rate

would increase the residence time of the particle in this region. If this same process occurred for many particles, than an increase in the below-canopy mean concentration would result thereby reducing the discrepancy seen in Fig. 3.

Another possible source of the discrepancy may be the use of an overly simplified (i.e. horizontally homogeneous, stationary) flow field, which lacks the sweeps and ejections that are ubiquitous with canopy flow. With a more realistic flow field, one in which the flow would be forced to split and form recirculating wake regions behind the obstacles, it is easy to envision particles becoming caught behind the obstacles for some time before carrying on downstream. This would increase the residence time of the particles in these regions and thus increase the below-canopy mean concentration, again reducing the discrepancy seen in Fig. 3. Sweeps would help bring material into the canopy, while ejections would carry material out. One step towards realism in the flow field that has been shown to not improve simulation predictions of the mean concentration field is the use of non-Gaussian velocity statistics (Flesch and Wilson 1992). The SPMMM–ID and Cassiani et al. (2007) simulation results support this finding.

Table 2 displays the performance measures of the mean concentration for both SPMMM simulations. From the performance measures, we see that both simulations have a tendency to underpredict the mean concentration ($FB > 0$). For the SPMMM–LD simulation, the fractional bias for the mean concentration is outside of the acceptable range. This is due to the within-canopy underprediction of the mean concentration at the $x/h_c = 0.38$ and $x/h_c = 2.78$ positions, as seen in Fig. 3. The other performance measures are within their acceptable ranges for both simulations, with the SPMMM–ID results being slightly more accurate.

The model results for vertical profiles of the dimensionless standard deviation of concentration are better, as seen in the Fig. 4. All the three simulations produced similarly good

Table 2 Performance measures for the SPMMM-simulated vertical profiles shown in Figs. 3 and 4

Statistic	Run	*FB*	*NMSE*	*FAC2*
$\langle\phi\rangle/\phi_*$ (Fig. 3)	SPMMM–ID	0.277	0.439	0.831
	SPMMM–LD	0.318	0.579	0.763
σ_ϕ/ϕ_* (Fig. 4)	SPMMM–ID	0.362	0.585	0.850
	SPMMM–LD	0.617	1.38	0.700

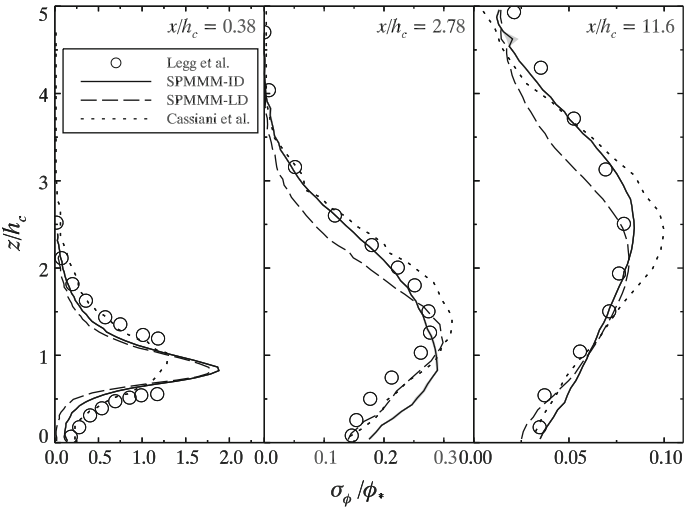

Fig. 4 Measured and modelled vertical profiles of the dimensionless standard deviation of concentration resulting from dispersion from a continuous, cross-wind line source ($z_s/h_c = 0.85$) in the Tombstone Canopy flow. The *circles* represent measurements from Legg et al. (1986). Three simulated profiles are shown: an SPMMM simulation utilizing a TKE dissipation rate inferred from T_L (*solid lines*), an SPMMM simulation utilizing a TKE dissipation rate calculated assuming local equilibrium (*dashed lines*), and the results of the Cassiani et al. (2007) model (*dotted lines*), which also used an inferred TKE dissipation rate

profiles. At the farthest measurement location $x/h_c = 11.6$, the SPMMM–ID simulation shows excellent agreement with the experimental data. As for the mean concentration results, the performance measures for the standard deviation of concentration (see Table 2) demonstrate both SPMMM simulations have reasonable performance. Both SPMMM–ID and SPMMM–LD simulations have unacceptably high fractional biases, which is due to the underprediction at the $x/h_c = 0.38$ position. The other performance measures are within their acceptable ranges for both simulations. As for the mean concentration results above, the SPMMM–ID simulation outperformed the SPMMM–LD simulation.

The results of the SPMMM and Cassiani et al. (2007) simulations suggest that concentration fluctuations, as with the mean concentration, can be simulated without taking the trouble to invoke more realistic, non-Gaussian velocity statistics, and this, to us, was initially quite surprising, given that it is generally argued that sweeps and ejections and micro-fronts dominate vertical transport of natural scalars (heat, vapour and CO_2) in a canopy. Two possible explanations for this are (1) the relative simplicity of the present source configuration (line source) permits neglect of the higher-order structure of the flow field, and (2) the one-point standard deviation of concentration does not contain much information about the higher-order

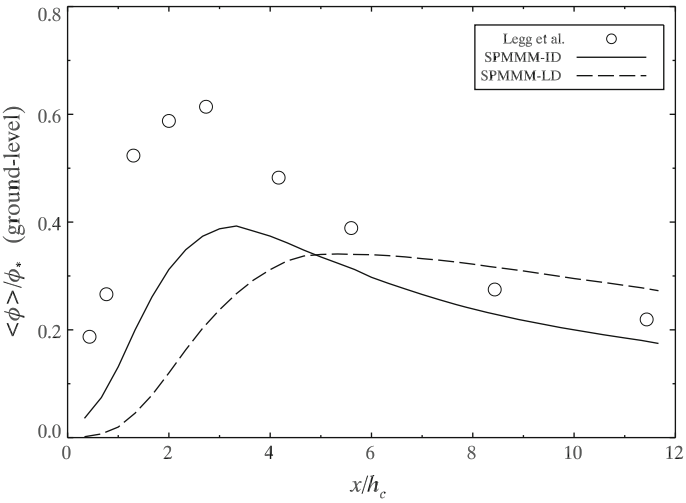

Fig. 5 Measured and modelled streamwise transects of the dimensionless ground-level concentration resulting from dispersion from a continuous, cross-wind line source ($z_s/h_c = 0.85$) in the Tombstone Canopy flow. The *circles* represent measurements from Legg et al. (1986). Two SPMMM-simulated profiles are shown: one utilizing a TKE dissipation rate inferred from T_L (*solid line*), the other utilizing a TKE dissipation rate calculated assuming local equilibrium (*dashed line*)

structure of the flow field. Perhaps higher-order moments such as the skewness and kurtosis of the concentration would be more sensitive to the representation of the velocity PDF.

Two streamwise transects of the ground-level dimensionless mean concentration as simulated by SPMMM are compared with experimental data in Fig. 5. For $x/h_c \lesssim 6$, the agreement is poor, with the mean concentration underpredicted by both SPMMM–ID and SPMMM–LD. The $x/h_c = 2.78$ panel in Fig. 3 displays the cause of these poor results. At this location, both the SPMMM–ID and the SPMMM–LD results have underpredicted the ground-level mean concentration. For $x/h_c \gtrsim 6$, the simulations agree better with the experimental data, with the SPMMM–ID results underpredicting the ground-level mean concentration, and the SPMMM–LD results overpredicting it. The SPMMM–ID simulation captures the shape of experimental transect of ground-level mean concentration better than the SPMMM–LD simulation, having a larger initial rise, and faster decay downstream. The performance measures for the ground-level mean concentration for these simulations are shown in Table 3. The SPMMM–ID simulation has a *FB* that is outside of the acceptable range, but with a *NMSE* and *FAC2* that are acceptable. Only the *NMSE* is acceptable for the SPMMM–LD simulation.

The SPMMM predictions for the streamwise transect of the concentration fluctuation intensity (defined here as $\max(\sigma_\phi)/\max\langle\phi\rangle$) shown in Fig. 6 are much better than the ground-level mean concentration. The performance measures for the concentration fluctuation intensity are shown in Table 3, and are very good for both simulations. Figure 4 shows that both the SPMMM–ID and SPMMM–LD simulations accurately predict the maximum concentration standard deviation. Figure 3 showed that the simulated maximum mean concentration is mostly underpredicted, except for the SPMMM–LD simulation at $x/h_c = 11.6$, where it is overpredicted. The overprediction of $\max(\sigma_\phi)/\max\langle\phi\rangle$ seen for both simulations in Fig. 6 is the result of the underprediction of $\max\langle\phi\rangle$. Furthermore, where the SPMMM–LD simulation overpredicted the maximum concentration at $x/h_c = 11.6$, the fluctuation intensity is

Table 3 Performance measures for the SPMMM simulated streamwise transects shown in Figs. 5 and 6

Statistic	Run	*FB*	*NMSE*	*FAC2*
$\langle\phi\rangle/\phi_*$ (Fig. 5)	SPMMM–ID	0.519	0.393	0.667
	SPMMM–LD	0.735	1.161	0.444
$\max(\sigma_\phi)/\max(\langle\phi\rangle)$ (Fig. 6)	SPMMM–ID	−0.224	0.0879	1.000
	SPMMM–LD	−0.039	0.0352	1.000

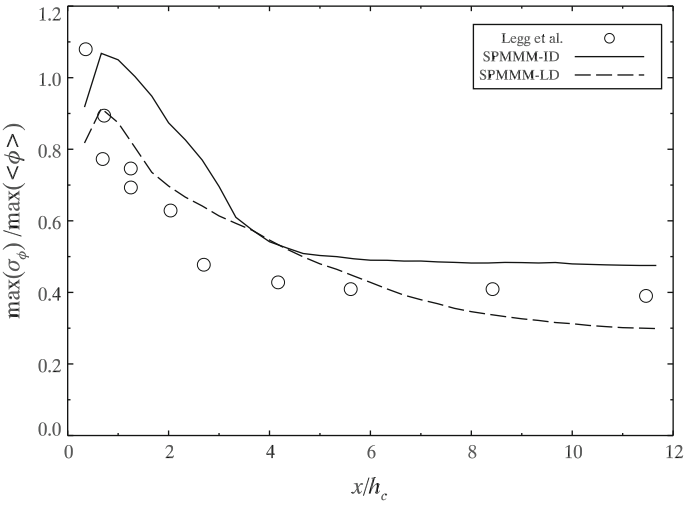

Fig. 6 Measured and modelled streamwise transects of the fluctuation intensity resulting from dispersion from a continuous, cross-wind line source ($z_s/h_c = 0.85$) in the Tombstone Canopy flow. The *circles* represent measurements from Legg et al. (1986). Two SPMMM simulated profiles are shown: one utilizing a TKE dissipation rate inferred from T_L (*solid line*), and the other utilizing a TKE dissipation rate calculated assuming local equilibrium (*dashed line*)

underpredicted. Taken together, the results shown in Figs. 5 and 6 imply that the SPMMM–ID and SPMMM–LD predictions of the streamwise transects of the first two concentration moments have fair accuracy.

5 Summary

It has been shown that SPMMM can with fair accuracy simulate dispersion within the Tombstone Canopy. The poorest predictions of SPMMM were for the mean concentration below the canopy, where SPMMM underpredicts the mean concentration (Figs. 3, 5). Predictions of the standard deviation of the concentration (Fig. 4) and the concentration were good, while predictions of fluctuation intensity (Fig. 6) were fair. Overall, the SPMMM–ID simulation, using a TKE dissipation rate inferred from the measured Lagrangian integral time scale profile and setting $C_0 = 2.0$, was more accurate than the SPMMM–LD simulation, which used a TKE dissipation rate that was the sum of shear and wake production of TKE, with $C_0 = 6.0$.

While the SPMMM–LD simulation had the poorest performance of the results displayed herein, we feel that the results were encouraging. There was no retuning of the free parameters from the values reported in Part I, which were optimized for a very different flow, and still SPMMM produced reasonably accurate predictions. From an emergency-preparedness standpoint, there is value in a model that once optimized requires no additional tuning and can make accurate predictions over a wide range of different types of flows. This value may simply be due to the ability to make quick, initial predictions to assist first-responders, while more accurate models which account for differences in source configuration and stability conditions are prepared.

The SPMMM–ID simulation was closer to the Cassiani et al. (2007) simulation (which also used a TKE dissipation rate inferred from the measured Lagrangian integral time scale profile and $C_0 = 2.0$), with small differences attributable to the implementation of the two models. It is conceivable that the SPMMM predictions could be improved upon by resolving the canopy obstacles and providing them reflection surfaces for the particles to reflect off, or by utilizing more realistic (inhomogeneous) flow statistics.

Both the SPMMM simulations, along with the simulation by Cassiani et al. (2007), support the findings of Flesch and Wilson (1992) and demonstrate that it is not necessary to invoke more realistic, non-Gaussian velocity statistics to simulate the mean concentration field in canopy flow with fair accuracy. In addition, the results presented herein show that this is also true for concentration fluctuations (in the situation examined); the assumption of Gaussian velocity statistics is sufficient for reasonably accurate predictions of the standard deviation of the concentration due to a line source in the Tombstone Canopy flow.

The results shown herein, along with those in Part I, demonstrate that the sequential particle trajectory with pre-calculation of the conditional means implementation used by SPMMM, and the simultaneous particle trajectory with on-the-fly calculation of the conditional means of the CASS implementation are effectively equivalent. If dispersion of reactive species is required, then the simultaneous particle trajectories must be used. However, for non-reactive species, it is advantageous to employ the sequential particle trajectory framework since the non-interactive nature of the particles allows for easy parallelization across multiple computer processors.

Acknowledgments This study was supported in part by grants from the Natural Sciences and Engineering Research Council of Canada (NSERC). The authors wish to thank the anonymous reviewers for their useful and constructive comments.

References

Brunet Y, Finnigan JJ, Raupach MR (1994) A wind tunnel study of air flow in waving wheat: single-point velocity statistics. Boundary-Layer Meteorol 70:95–132

Cassiani M, Franzese P, Giostra U (2005) A PDF micromixing model of dispersion for atmospheric flow. Part I: development of model, application to homogeneous turbulence and to a neutral boundary layer. Atmos Environ 39:1457–1469

Cassiani M, Radicchi A, Albertson JD (2007) Modelling of concentration fluctuations in canopy turbulence. Boundary-Layer Meteorol 122:655–681

Chang CJ, Hanna SR (2004) Air quality performance evaluation. Meteorol Atmos Phys 87:167–196

Coppin PA, Raupach MR, Legg BJ (1986) Experiments on scalar dispersion within a model plant canopy. Part 2: An elevated plane source. Boundary-Layer Meteorol 35:167–191

Fackrell JE, Robins AG (1982) Concentration fluctuations and fluxes in plumes from point sources in a turbulent boundary layer. J Fluid Mech 117:1–26

Flesch TK, Wilson JD (1992) A two-dimensional trajectory-simulation model for non-Gaussian, inhomogeneous turbulence within plant canopies. Boundary-Layer Meteorol 61:349–374

Fox RO (1996) On velocity-conditioned scalar mixing in homogeneous turbulence. Phys Fluids 8:2678–2691
Franzese P (2003) Lagrangian stochastic modelling of a fluctuating plume in the convective boundary layer. Atmos Environ 37:1691–1701
Franzese P, Cassiani M (2007) A statistical theory of turbulent relative dispersion. J Fluid Mech 571:391–417
Legg BJ, Raupach MR, Coppin PA (1986) Experiments on scalar dispersion within a model plant canopy. Part 3: An elevated line source. Boundary-Layer Meteorol 35:277–302
Luhar AK, Sawford BL (2005) Micromixing modelling of concentration fluctuations in inhomogeneous turbulence in the convective boundary layer. Boundary-Layer Meteorol 114:1–30
Monin AS, Yaglom AM (1975) Statistical fluid mechanics II. MIT Press, Cambridge, 874 pp
Poggi D, Katul GG, Cassiani M (2008) On the anomalous behaviour of the Lagrangian structure function similarity constant inside dense canopies. Atmos Environ 42:4212–4231
Pope SB (1998) The vanishing effect of molecular diffusivity on turbulent dispersion: implications for turbulent mixing and the scalar flux. J Fluid Mech 359:299–312
Postma JV, Wilson JD, Yee E (2011) Comparing two implementations of a micromixing model. Part I: Wall shear-layer flow. Boundary-Layer Meteorol. doi:10.1007/s10546-011-9605-5 (this issue)
Raupach MR, Coppin PA, Legg BJ (1986) Experiments on scalar dispersion within a model plant canopy. Part 1: The turbulence structure. Boundary-Layer Meteorol 35:21–52
Raupach MR, Coppin PA, Legg BJ (1987) Erratum: Experiments on scalar dispersion within a model plant canopy. Part 1: The turbulence structure. Boundary-Layer Meteorol 39:423–434
Rembold B, Grass M, Jenny P (2008) Parallel hybrid particle/finite volume algorithm for transported PDF methods employing sub-time stepping. Comput Fluids 37(3):181–193
Sawford BL (2004) Micro-mixing modelling of scalar fluctuations for plumes in homogeneous turbulence. Flow Turbul Combust 72:133–160
Thomson DJ (1987) Criteria for the selection of stochastic models of particle trajectories in turbulent flows. J Fluid Mech 180:529–556
Thomson DJ (1996) The second-order moment structure of dispersing plumes and puffs. J Fluid Mech 320:305–329